

1 **Hydraulic Redistribution Decreases with Precipitation Magnitude and Frequency in a**
2 **Dryland Ecosystem: A Data-Model Fusion Approach**

3 Aneesh Kumar Chandel¹, Mitra Cattray³, Yu Zhou⁴, Hang Duong^{2,5}, Marcy Litvak², William
4 Pockman² and Yiqi Luo¹

5 ¹School of Integrative Plant Science, Cornell University, Ithaca, NY, USA

6 ²Biology Department, University of New Mexico, Albuquerque, NM, USA

7 ³Department of Earth and Environmental Engineering, Columbia University, USA

8 ⁴Department of Environmental Systems Science, ETH Zurich, Switzerland

9 ⁵Vietnam National University of Agriculture, Hanoi, Vietnam

10 Corresponding Authors: Aneesh Kumar Chandel (akc76@cornell.edu), Yiqi Luo

11 (y12735@cornell.edu)

12

13

14

15

16

17

18

19

20

Formatted: Not Superscript/ Subscript

21 **Abstract**

22 Hydraulic redistribution (HR), the movement of water via plant root systems that connect soil
23 compartments with different water potential, should ~~influences~~influence soil moisture dynamics
24 particularly in ~~dryland water limited~~ ecosystems, where water availability strongly constrains
25 ecosystem function. Realistic representation of HR in ecosystem models is essential to improve
26 the ability of these models to predict ecosystem function in dryland regions. In this study, we
27 integrated HR into the Terrestrial ECOsystem model and employed a Bayesian Markov Chain
28 Monte Carlo technique to optimize soil hydraulic parameters and root conductance using four
29 years of soil moisture observations from a piñon-juniper woodland. We found that (i) integrating
30 HR generally improved model prediction of soil moisture during dry periods, particularly in the
31 top 30 cm of the soil profile, where more than 50% of root biomass exists, ~~mostly during dry~~
32 ~~periods~~; (ii) HR increased surface soil moisture by up to 60% during dry periods; (iii) HR
33 decreased with increasing precipitation magnitude and frequency, however, the length of dry
34 spells between rainfall events also influenced HR rates; and (iv) upward HR in the top 60 cm soil
35 profile became more pronounced as dry conditions progressed, with rates ranging from 0.10 to
36 0.50 mm d⁻¹. These findings highlight that HR plays a likely-critical role in sustaining soil
37 moisture during extended dry periods and has a limited effect during precipitation events. Future
38 research should investigate the effect of HR on other ecosystem processes, such as net ecosystem
39 exchange of carbon and evapotranspiration under varying climatic conditions.

40

41

42

Formatted: Superscript

43

44 1. Introduction

45 Soil volumetric water content (VWC), defined as the amount of water stored in the
46 unsaturated zone of the soil profile, is a fundamental state variable regulating ecosystem water
47 and energy exchanges, particularly in dryland ecosystems (Seneviratne et al., 2010). Drylands,
48 cover over 40% of Earth's terrestrial surface and support more than 38% of the global population
49 (Průhová, 2016), underscoring the importance of understanding soil moisture dynamics in these
50 regions. While VWC provides a useful measure of soil water status, the movement and
51 availability of this water are governed by soil water potential, particularly its matric component,
52 which reflects the capillary and adsorptive forces binding water to soil particles (Hillel, 2003;
53 Novick et al., 2022). In unsaturated soils, matric potential determines how tightly water is
54 retained and how readily it can move toward plant roots. Because Ecosystem function in these
55 dryland ecosystem functioning regions is likely strongly constrained, to be limited by altered
56 precipitation variability in the changing climate (Beer et al., 2010; Ukkola et al., 2021).
57 ~~Understanding how plants regulate water under fluctuating moisture conditions is essential the~~
58 ~~ability of plants to mitigate the potential negative impacts of alter precipitation is therefore~~
59 ~~critical~~ for predicting ecosystem stability.

60 One key mechanism underlying this regulation is ~~H~~hydraulic redistribution (HR), is the
61 passive movement of water through plant roots, usually at night, from wet to dry regions of the
62 plant rooting volume driven by differences in water potential. This passive process can favor
63 plant survival during droughts by tapping into deep soil layers having relatively higher water
64 potential and redistributing water to the shallow root zone (upward HR) (Nadezhdina et al.,
65 2015; Prieto et al., 2012; Nicola and Ram, 2022). During wet seasons, HR can redistribute water

66 from wet surface soil into deeper, drier soil (downward HR), supplementing the infiltration
67 process in recharging deeper soil layers (Hultine et al., 2003; Scott et al., 2008; Fu et al., 2016;
68 Bleby et al., 2010). Despite its potential role in regulating plant and ecosystem productivity,
69 nutrient cycling and soil microbial activity (Grünzweig et al., 2022; Sardans and Peñuelas,
70 2014), most current dynamic global vegetation models and Earth system model still lack an
71 explicit representation of HR-is often ignored in ecosystem models (Fu et al., 2016).
72 ~~HR hydraulic redistribution~~ has been observed across diverse ecosystems and plant species
73 (Neumann and Cardon, 2012; Nadezhkina et al., 2010; Yu et al., 2013; Priyadarshini et al.,
74 2016). It is recognized as a structural driver of ,and has been interpreted as structuring dryland
75 plant communities, regulating ecosystem productivity, and enhancing resilience to climate
76 extremes (Lee et al., 2018; Barron - Gafford et al., 2021; Barron - Gafford et al., 2017; Hafner et
77 al., 2020). The dynamics of HR are influenced by various biotic (rooting architecture, plant
78 capacitance, transpiration demand, senescence, and dormancy), abiotic factors (soil hydraulic
79 characteristics, soil moisture status), and climatic conditions (precipitation) (Prieto et al., 2012;
80 Katul and Siqueira, 2010; Wei et al., 2022). While several studies ~~have examined HR in deserts~~
81 ~~arid and semi-arid ecosystems~~ have and reported upward HR during dry ~~events periods~~ (Hao
82 et al., 2013a; Lee et al., 2018; Scott et al., 2008; Yu et al., 2013) and downward HR following
83 precipitation ~~(Hultine et al., 2003), studies focusing on the~~ fine-scale temporal ~~variations~~
84 ~~variability of~~ HR across ~~multiple different~~ soil depths and multi-~~ple~~-year ~~timescales~~ remains
85 limited. ~~Additionally~~ ~~Moreover~~, a quantitative understanding of how precipitation magnitude and
86 frequency ~~influence HR rates~~, key limiting factors in dryland ecosystems, influence HR rates
87 ~~remain is still lacking~~ ~~poorly understood~~.

88 In this study, we explicitly test two hypotheses: (1) Direction of HR: Upward HR should be
89 the dominant form of HR in dryland ecosystem. This is due to the recharge of deeper soil layers
90 from precipitation which can retain moisture for longer periods, and during dry periods roots
91 facilitate the movement of this retained water to the drier surface soils. (2) HR-precipitation
92 relationship: Uppward HR should decline following precipitation events, reaching its maximum
93 rates during prolonged dry periods as ~~the~~ drought ~~ereate~~creates steep water potential gradients
94 between deeper, moist soil layers and the drier surface layers, facilitating the upward ~~movement~~
95 redistribution of water.

96 Meanwhile, ~~S~~oil moisture dynamics are governed by a complex interplay of forces that
97 drive water movement through the soil profile. The primary drivers include matric
98 potential (capillary and adsorptive forces binding water to soil particles), gravitational
99 potential (driving downward drainage), and ~~potential gradients that induce processes like~~ HR
100 (Caldwell et al., 1998). These forces collectively determine soil water retention, redistribution,
101 and plant water availability (Hillel, 2003). However, ~~i~~solating their individual contributions
102 from field soil moisture ~~data observations~~ is challenging, ~~as because these processes operate~~
103 simultaneously and their effects are strongly influenced ~~concurrent and modulated~~ by soil
104 properties, root activity, and atmospheric conditions. Consequently, a data-model fusion
105 approach, which ~~integrates~~ing process-based ~~model~~models with soil moisture ~~data~~observations,
106 provides a robust framework to isolate and quantify HR, offering a more mechanistic and
107 quantitative understanding of soil-plant water dynamics.

108 Several modeling studies have incorporated various HR schemes into process-based models
109 to improve understanding of hydrological and ecological processes (Ryel et al., 2002; Amenu
110 and Kumar, 2008; Wu et al., 2020; Fu et al., 2016; Zheng and Wang, 2007; Tang et al., 2015;

111 Lee et al., 2018; Quijano and Kumar, 2015). However, realistic representation and estimation of
112 parameters related to HR remains a challenge, as neither the magnitude of HR nor its associated
113 parameters can be directly observed in the soil (Ryel et al., 2002; Quijano and Kumar, 2015). As
114 a result, most models rely on default HR parameter values derived from Ryel et al. (2002). For
115 example, in a study by Fabian et al. (2010), the maximum soil-root radial conductance (C_{RT}), a
116 key parameter controlling HR, was assigned as the mean value between C_{RT} reported by ~~Ryel,~~
117 ~~2002 #532~~ Ryel et al. (2002) for *Artemisia tridentata* and by Williams et al. (1996) for *Quercus-*
118 *Acer* stand. Similarly, Zheng and Wang (2007) and Yan and Dickinson (2014) prescribed a
119 constant C_{RT} value based on Ryel et al. (2002). Alternatively, some studies ~~(Fabian et al., 2010;~~
120 ~~Zheng and Wang, 2007) or~~ ~~(Fu et al., 2016)(Fu et al., 2018b)~~ estimated parameters using soil
121 moisture data during specific periods of time when upward or downward HR is assumed
122 negligible, such as wet or dry season (Fu et al., 2018; Fu et al., 2016) ~~(Amenu and Kumar, 2008;~~
123 ~~Yan and Dickinson, 2014; Fu et al., 2016; Fu et al., 2018)~~. These challenges in direct
124 measurements, the ~~and~~ reliance on assumed parameter values, and the parameterization of HR
125 under the assumption of negligible redistribution, ~~–~~ constitute key gaps in our understanding of
126 HR dynamics.

127 To address these gaps, we focused on piñon-juniper (PJ) woodlands, the most widespread
128 semi-arid ecosystem in the US. PJ woodlands are spatially widespread, ecologically important,
129 temporally dynamic, and structurally unique dryland ecosystem in the western US, spanning 10
130 US states and 40 million hectares across the American Southwest (Eastburn et al., 2024; Romme
131 et al., 2009). Despite their importance, HR has not been previously ~~reported~~ studied in PJ
132 woodlands. However, our continuous root sap flux measurements provided direct evidence of

Formatted: Font: Italic

Formatted: Font: Italic

Formatted: Font: Italic

Formatted: Font: Not Italic

Formatted: Font: Italic

133 HR in both piñon and juniper roots, indicated by sustained negative root sap flux during
134 nighttime at the study site (Fig. S-1).

135 In this study, we used the process-based Terrestrial Ecosystem (TECO) model to (i) develop
136 and implement a data assimilation approach to ~~incorporate~~integrate HR into the TECO model;
137 (ii) quantify and characterize the magnitude and dynamics of HR across multiple soil depths; and
138 (iii) analyze the temporal patterns of HR and its relationship with precipitation magnitude and
139 frequency. The TECO model is a well-established ecosystem model that integrates ecological
140 processes to simulate carbon, water, and energy fluxes within terrestrial ecosystems (Weng and
141 Luo, 2008). We employed data assimilation to constrain the TECO model including HR using
142 four years of soil moisture data measured at multiple soil depths, encompassing both wet and dry
143 periods.

144 2. Data and Methods

145 2.1 Study site and data

146 Our modeling study utilized data from a PJ woodland plot (Lat. 35.642, Long. -104.607,
147 elevation 1925 m) located in New Mexico, USA, and previously described in Schwinning et al.
148 (2020). The site is a private ranch covering an area of over 6800 hectares that was ungrazed
149 from 2012 through the measurement period used for this study and is characterized by a semi-
150 arid climate. Mean annual precipitation of the site is approximately 460 mm, with the majority
151 falling between May and October, and a mean annual temperature of 10.5 °C. The soil texture at
152 the site varies with depth, ranging from loam to clay loam. The vegetation consists of distinct
153 tree clusters dominated by piñon pine (*Pinus edulis* (Englem.)) and juniper (*Juniperus*
154 *monosperma* (Englem.) Sarg.) separated by open areas of bare soil and herbaceous cover.

155 ~~SWC-VWC~~ was continuously monitored using multi-sensor frequency domain capacitance
156 probes (Decagon EC-5) installed at four depths (5, 15, 30 and 60 cm), in four soil pits under the
157 tree canopies. All sensors were monitored every minute by a datalogger (model CR6, Campbell
158 Scientific), ~~storing and~~ 15-minute averages were stored ~~by a data logger~~. For ~~model~~
159 ~~parameterization, we used 15-min VWC records aggregated to daily means~~ ~~this study, we used~~
160 ~~the average SWC across all four pits~~. Each sensor was calibrated in the lab before installation for
161 both air and water frequency. ~~Because Significant shifts in~~ soil temperature can affect both soil
162 permittivity and the response of capacitance sensors, potentially confounding the small
163 fluctuations in VWC caused by HR. ~~Therefore~~, temperature correction factors were applied to
164 the measured VWC at each depth, using the nearest measured temperature, following the method
165 described by Saito et al. (2009). ~~Rather than excluding data below 0 °C, we used this~~
166 ~~temperature-correction approach to reduce the influence of temperature-driven artifacts on the~~
167 ~~soil moisture signal. This strategy allows retention of continuous soil moisture records while~~
168 ~~accounting for the known sensitivity of capacitance sensors to temperature-dependent changes in~~
169 ~~dielectric permittivity.~~

170 2.2 Modeling framework

171 TECO is a process-based ecosystem model (Hou et al., 2021; Jiang et al., 2018; Weng and
172 Luo, 2008), and has evolved from the TCS model (Luo and Reynolds, 1999). The model ~~consists~~
173 ~~of has four~~ major components: canopy photosynthesis, plant growth, soil water dynamics, and
174 soil carbon transfers. The canopy photosynthesis and soil water dynamics submodels run at the
175 hourly time step whereas the plant growth and soil carbon submodels run at the daily time step.
176 The model is driven by seven environmental variables, including precipitation (mm), wind speed
177 (m s^{-1}), solar radiation (W m^{-2}), air and soil temperature (C), relative humidity (%), and vapor

178 pressure deficit (kPa). The detailed description of TECO model is available (Weng and Luo,
179 2008) and only ~~the~~ brief description of soil water dynamics is provided here.

180 The soil profile is divided into 10 layers with a total depth of 180 cm, with varying thickness:
181 5 cm for the first layer, 10, 15, and 30 cm for the second, third, and fourth layers respectively,
182 and 20 cm for each of the fifth ~~through~~ tenth layers. VSWC in each layer results from the mass
183 balance between influx and efflux, with changes primarily attributed to vertical unsaturated flow,
184 transpiration, precipitation, runoff, and drainage. Evaporation depletes water from the first two
185 soil layers, while transpiration depletes water from all soil layers containing roots, allocated
186 based on root fraction in each layer (Eq. 8). Given the predominantly arid conditions of the study
187 site, runoff and drainage were found negligible. Thus, water movement between soil layers is
188 simulated as follows:

$$189 \quad \frac{dW_i}{dt} = \frac{dF_i}{dz} - E_i - T_i \quad (1)$$

190 where W_i is the water storage (cm) in layer i , t is time (h), F_i is net unsaturated flow of water into
191 layer i (cm h^{-1}), z is vertical thickness, E_i and T_i are evaporation and transpiration water loss from
192 layer i (cm h^{-1}).

193 The unsaturated soil water movement is simulated vertically according to modified form of
194 Buckingham-Darcy's law (Campbell, 1985) (Eq. 2), with Brooks (1965) equation (Eq. 4)
195 estimating hydraulic conductivity and soil water retention curve (SWRC) to simulate soil water
196 potential (Ψ).

$$197 \quad \frac{dF_i}{dz} = K(\theta_i) \left(\frac{d\Psi_i}{dz} + 1 \right) \quad (2)$$

198 where $K(\theta_i)$ is the unsaturated soil hydraulic conductivity (cm h^{-1}) for VSWC θ ($\text{cm}^3 \text{cm}^{-3}$) in
199 layer i , Ψ_i is soil water matric potential (MPa) in layer i , and z is the vertical thickness (cm) of
200 the soil.

Formatted: Font: Italic

201
$$K(\theta_i) = K_s \left[\frac{\theta_i - \theta_r}{\theta_s - \theta_r} \right]^{(2m+3)} \quad (3)$$

202 where, K_s is the soil saturated hydraulic conductivity (cm h^{-1}), m is the pore size distribution
 203 index, θ_s and θ_r are saturated and residual VSWC ($\text{cm}^3 \text{ cm}^{-3}$)

204
$$\frac{\theta - \theta_r}{\theta_s - \theta_r} = \left(\frac{\Psi}{\Psi_b} \right)^{-1/m} \quad (4)$$

205 Ψ_b is the soil air entry water potential.

206 To quantify the direction and magnitude of HR, we integrated the HR model by Ryel et al.
 207 (2002) into equation 1 of TECO model (~~presented in equation Eq. 5~~). This HR model empirically
 208 describes HR flux based on the soil water potential gradient between two soil layers (Eq. 6). HR
 209 was assumed to occur only at night, with its occurrence controlled by solar radiation instead of
 210 fixed day and night hours. Daytime starts as solar radiation exceeds 10 W m^{-2} , thereby inhibiting
 211 HR since the water potential gradient typically favors water movement from roots to canopy to
 212 meet transpiration demand during the day. This pattern is evident in Fig. S1, where under low or
 213 zero solar radiation, root sap flux was found to be negative, indicating water movement away
 214 from the root zone which is an indicator of occurrence of HR at the study site. Using these
 215 assumptions, the net water movement into soil layer i from other soil layers j can be expressed
 216 as:

217
$$\frac{dW_i}{dt} = \frac{dF_i}{dz} - E_i - T_i + H_i \quad (5)$$

218
$$H_i = C_{RT} \sum (\Psi_j - \Psi_i) \max(c_i, c_j) \frac{R_i R_j}{1 - R_x} D_{tran} \quad (6)$$

219
$$c_i = \frac{1}{1 + \left(\frac{\Psi_i}{\Psi_{50}} \right)^b} \quad (7)$$

220
$$R_i = \frac{R_0}{1 + \left(\frac{d}{d_{50}} \right)^a} \quad (8)$$

Formatted: Not Superscript/ Subscript

Formatted: Font: Italic

221 ~~w~~Where in Eq 6, H_i is the net water redistributed by roots into layer i (cm h^{-1}) ~~from other soil~~
 222 ~~layers~~ j , C_{RT} is the maximum radial soil-root conductance of the entire active root system for
 223 water ($\text{cm MPa}^{-1} \text{h}^{-1}$), Ψ is soil matric potential (MPa), c_i is a factor reducing soil-root
 224 conductance based on Ψ_i , R_i is the fraction of active roots in layer i , R_0 is the average vertically
 225 summed root dry mass from the bottom to the root zone to the soil surface, and D_{tran} is a factor
 226 reducing water movement among layers by roots while plant is transpiring and is assumed to be
 227 $1-\theta$ during the night when transpiration is minimal and $0-\theta$ during day. $R_x = R_i$ when $\theta_i > \theta_j$ or R_x
 228 $= R_j$ when $\theta_j > \theta_i$. In Eq 7, Ψ_{50} is the soil water potential (MPa) where conductance is reduced by
 229 50% and b is an empirical constant. In Eq 8, d is soil depth (cm), and d_{50} is the soil depth at the
 230 median of the root distribution and a is a shape parameter (Table 1). The Brooks (1965) model
 231 for SWRC was utilized to simulate soil water potential (Ψ), facilitating the development of soil
 232 water potential gradients necessary for HR by tree roots (Eq. 4). Due to lack of site-specific
 233 parameters, the default values of b and Ψ_{50} were used as 3.22 and -1 MPa, respectively (Ryel et
 234 al., 2002).

Formatted: Font: Italic

Formatted: Font: Italic

Formatted: Font: Italic

Formatted: Font: Italic

235 2.3 Data assimilation for parameters estimation

236 We used Bayesian probabilistic inversion to calibrate parameters associated with soil
 237 hydraulics, where posterior probability density functions of parameters are obtained from prior
 238 knowledge about the parameters and the error between model and observations. According to
 239 Mosegaard and Sambridge (2002), Bayesian inversion can be summarized by the following
 240 equation:

$$241 \quad p(c|Z) \propto p(Z|c) p(c) \quad (9)$$

242 where $p(c|Z)$ is posterior probability density function of model parameters c ; $p(Z|c)$ is a
 243 likelihood function of parameters c ; $p(c)$ is prior probability density function of parameters c . We

244 assumed that the prediction errors were normally distributed and uncorrelated, hence, the
 245 likelihood function, $p(Z|c)$, was calculated as follows:

$$246 \quad p(Z|c) \propto \exp\left\{-\sum_{i=1}^k \frac{(Z_i - X_i)^2}{2\sigma_i^2}\right\} \quad (10)$$

247 where Z_i is observed VWC at i^{th} soil layer, X_i is VWC simulated by TECO at a corresponding
 248 soil depth; σ_i^2 is the variance of a measurement at a soil layer; k is the total number of soil layers.

249 To generate the posterior distributions, we first specified the priors of the parameters to be
 250 uniformly distributed over the intervals specified in Table 1. We put constraints on parameters
 251 based on ~~the literature~~ literature. The initial set of parameters was randomly selected within the
 252 prior parameter ranges. Once we specified parameter ranges, we used the Metropolis-Hastings
 253 (M-H) algorithm (Hastings, 1970; Metropolis et al., 1953), a Markov chain Monte Carlo method,
 254 to sample from the posterior parameter distribution. To generate a parameter set, we ran M-H
 255 algorithm in two steps: proposing step and ~~a moving~~ moving step. In the proposing step, a new
 256 parameter set c^{new} was generated from a previously accepted parameter set c^{k-1} through a
 257 proposal distribution ($c^{\text{new}}|c^{k-1}$):

$$258 \quad c^{\text{new}} = c^{k-1} + r \times \frac{c^{\text{max}} - c^{\text{min}}}{D} \quad (11)$$

259 The value of $P(c^{k-1}|c^{\text{new}})$ was then compared with a random number U from 0 to 1. Parameter set
 260 c^{new} was accepted if $P(c^{k-1}|c^{\text{new}}) \geq U$, otherwise c^k was set to c^{k-1} . In the moving step, a
 261 probability of acceptance $P(c^{k-1}|c^{\text{new}})$ was calculated as in the following (Marshall et al., 2004):

$$262 \quad P(c^{k-1}|c^{\text{new}}) = \min\left\{1, \frac{p(Z|c^{\text{new}})p(c^{\text{new}})}{p(Z|c^{k-1})p(c^{k-1})}\right\} \quad (12)$$

263 The M-H algorithm was repeated for 50,000 simulations, and then all accepted parameters
264 values were used to generate the probability distribution functions (Xu et al., 2006). ~~Finally,~~
265 ~~before each model simulation with optimized parameters, we ran the model for 200 years, a spin-~~
266 ~~up period that was long enough to obtain stable carbon stock as an initial condition for these~~
267 ~~simulations.~~

268 To evaluate the impact of HR on soil moisture dynamics in a PJ woodland, we conducted
269 two multi-year simulations using two configurations of the TECO model: TECO+HR (with HR)
270 and default TECO (HR turned off). To distinguish the influence of HR from soil hydraulic
271 properties, we adopted a data assimilation approach focused on calibrating only the TECO+HR
272 model. Soil moisture observations were available at 5, 15, 30 and 60 cm depths, and data
273 assimilation was therefore applied only to these four soil layers over a four-year period, and data-
274 model comparisons are presented exclusively for these depths. The parameters values deeper
275 than 60 cm were not calibrated and were empirically defined from literature values. This
276 modeling strategy is consistent with other data assimilation studies, in which model calibration is
277 restricted to soil layers with available observations (Fu et al., 2016; Zhang et al., 2016). ~~We~~
278 ~~calibrated TECO+HR model using soil moisture data measured at 5, 15, 30, and 60 cm depths~~
279 ~~over a four year period.~~ In total, 21 parameters were optimized including 20 soil hydraulic
280 parameters (θ_s , θ_r , K_s , m , and Ψ_b for each of the four soil depths) across four soil layers and one
281 HR-related parameter (C_{RT}). The prior range of soil hydraulic parameters were informed by
282 established relationships between soil texture and hydraulic properties (Rawls et al., 1982; Clapp
283 and Hornberger, 1978). The prior range for C_{RT} was based on values reported in Fu et al. (2016).
284 prior parameter values was informed by available soil texture data for the study site (Carsel and

Formatted: Font: Italic

Formatted: Font: Italic, Subscript

Formatted: Font: Italic

Formatted: Font: Italic, Subscript

Formatted: Font: Italic

Formatted: Font: Italic, Subscript

Formatted: Font: Italic

Formatted: Font: Italic

Formatted: Font: Italic, Subscript

Formatted: Font: Italic

Formatted: Font: Italic, Subscript

285 ~~Parrish, 1988; Brooks, 1965~~). Within this range, we optimized depth-specific soil hydraulic
286 parameters to achieve a close match between modeled and observed soil moisture (Table 1).

287 After calibrating the TECO+HR model, we deactivated the HR process and ran simulations
288 with the same optimized parameters to generate the default TECO scenario. Before each model
289 simulation, we performed a 200-year spin-up separately for both model configuration
290 (TECO+HR with HR active and default TECO with HR disabled) to ensure that each model
291 reached stable carbon stocks as initial conditions.

292 ~~This approach allowed us to ensure that differences in soil moisture dynamics between~~
293 ~~TECO+HR and default TECO simulations were attributable solely to the presence or absence of~~
294 ~~HR.~~ ~~The~~ motivation to calibrate only TECO+HR model, rather than the default TECO is to
295 avoid parameter compensation for unresolved processes (Luo and Schuur, 2020), in which the
296 absence of HR could lead to unrealistic adjustments of soil hydraulic parameters to indirectly
297 capture its effects. This approach allowed us to ensure that differences in soil moisture dynamics
298 between TECO+HR and default TECO simulations were attributable solely to the presence or
299 absence of HR.

300 Furthermore, to evaluate the influence of cumulative precipitation and soil moisture memory
301 on HR, we calculated the Antecedent Precipitation Index (API) for the study period (2018–2021)
302 following Kohler and Linsley (1951). API acts as a proxy for soil moisture status by accounting
303 for the decaying effect of past rainfall events. The daily API (API_t) was calculated using the
304 recursive decay function:

305
$$API_t = P_t + (k * API_{t-1}) \quad (13)$$

- Formatted: Font: Italic
- Formatted: Font: Italic, Subscript
- Formatted: Font: Italic
- Formatted: Font: Italic, Subscript
- Formatted: Font: Italic
- Formatted: Font: Italic, Subscript
- Formatted: Font: Italic
- Formatted: Font: Italic, Subscript
- Formatted: Font: Italic
- Formatted: Font: Not Italic
- Formatted: Centered, Indent: Left: 1.5", First line: 0.5"

306 where P_t is the precipitation on day t (mm), API_{t-1} is the index value of the preceding day,
307 and k is a decay constant representing the recession of soil moisture due to evapotranspiration
308 and drainage. We used a decay constant of $k = 0.90$, which falls within the commonly applied
309 range for antecedent precipitation indices and is consistent with optimization analyses indicating
310 optimal decay constants near 0.90 (Li et al., 2021). This metric enables differentiation between
311 short dry intervals following wet conditions and extended dry spells with limited antecedent
312 moisture.

Formatted: Font: Italic

Formatted: Font: Italic, Subscript

Formatted: Font: Italic

Formatted: Font: Italic

Formatted: Font: Italic, Subscript

Formatted: Normal

Formatted: Font: Italic

Formatted: Font: Italic

313 2.4 Statistical ~~analyses~~analysis

314 Model performance was assessed by comparing simulated outputs with observed data during
315 full simulation periods (2018- 2021), dry, and wet periods, defined as days without and with
316 rainfall events, respectively. During the study period, wet days accounted for 22% of all days,
317 whereas dry days comprised the remaining 78%. Model performance was evaluated using two
318 statistical metrics: root mean square error (RMSE) and absolute mean error (MAE). RMSE is
319 widely used to quantify model accuracy, but its squared-error formulation overemphasizes the
320 effects of large deviations (Willmott and Matsuura, 2005). Therefore, MAE was also calculated
321 as a measure of the average magnitude of deviation from observed values (Alfieri et al., 2017).
322 Both metrics were calculated as follows: Evaluation was conducted using statistical metrics,
323 including root mean square error (RMSE), and absolute mean error (MAE).

Formatted: Font:

$$324 \quad RMSE = \sqrt{\frac{1}{n} \sum_{i=1}^n (m_i - o_i)^2} \quad (143)$$

$$325 \quad MAE = \frac{1}{n} \sum_{i=1}^n |m_i - o_i| \quad (154)$$

326 Where: o_i represents observed values, m_i represents modeled values, and n represents the
327 number of data points.

Table 1: Parameters constrained using data assimilation in the TECO model from soil moisture data from 2018 to 2021.

Parameters	Symbols	Constrained values	Range	Units	References
Saturated water content	θ_s	0.34/0.38/0.36/0.33	[0.3, 0.4]	$\text{cm}^3 \text{cm}^{-3}$	Calibrated
Residual water content	θ_r	0.05/0.07/0.06/0.03	[0, 0.08]	$\text{cm}^3 \text{cm}^{-3}$	Calibrated
Saturated hydraulic conductivity	K_s	0.14/0.29/0.30/0.70	[0.1, 2]	cm h^{-1}	Calibrated
Pore size distribution	m	0.89/0.66/0.88/0.84	[0, 1]	-	Calibrated
Air entry water potential	Ψ_b	96/60/50/40	[0, 100]	cm	Calibrated
Maximum radial soil-root conductance	C_{RT}	0.022	[0, 1]	$\text{cm MPa}^{-1} \text{h}^{-1}$	Calibrated
Soil Ψ where root conductivity reduced by 50%	Ψ_{50}	-1.0	-	MPa	(Ryel et al., 2002)
Empirical constant	b	3.22	-	-	(Ryel et al., 2002)
Average vertically summed root dry mass	R_0	0.90	-	kg m^{-2}	(Schwinning et al., 2020)
Soil depth at the median of the root distribution	D_{50}	25	-	cm	(Schwinning et al., 2020)
Root distribution shape parameter	a	2.2	-	-	(Schwinning et al., 2020)

Four values represent parameters in the four modeled Ψ WC at depths of 5, 15, 30, and 60 cm, respectively.

330 **3. Results**

331 **3.1 Parameter estimation via data assimilation and water mass balance**

332 The data assimilation approach, using ~~observational~~ VSWC data to constrain the model,
333 yielded well-constrained soil hydraulic parameters (Table 1; Fig. S2 and S3). The resulting
334 posterior probability density functions, characterized by sharp peaks, narrow spread, and
335 consistency across soil depth support the reliability and accuracy of these calibrated parameter
336 values. Additionally, soil water mass balance of soil profile was conserved before and after
337 incorporating the HR process into the TECO model (Fig. S4). The key components of the water
338 budget: precipitation, evapotranspiration, and changes in soil water content remained balanced,
339 ensuring that the model accounted for all water fluxes. Furthermore, the sum of HR across all
340 soil layers (10 layers) was consistently equal to zero, further ensuring that no water was
341 artificially introduced or lost from the system.

342

343

344

345

346

347

348

349

350

351 **3.2 Observed and simulated soil moisture**

352 ~~3.2~~

Formatted: Font: Not Bold

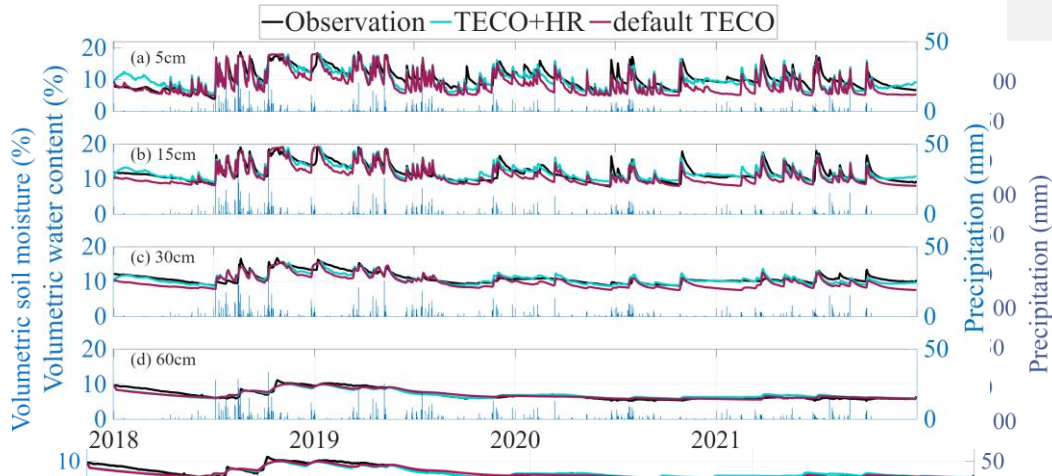


Figure 1a-d: Observed and simulated soil volumetric water content for the year 2019 (January 1, 2018 to December 31, 2021) at soil depths of 5 cm (a), 15 cm (b), 30 cm (c), and 60 cm (d). Black lines indicate observations, cyan lines indicate TECO+HR, and magenta lines indicate default TECO. Vertical blue bars indicate daily precipitation (right axis).

353

354

355

356

357

358

359

360

361

362

363

364

365

366

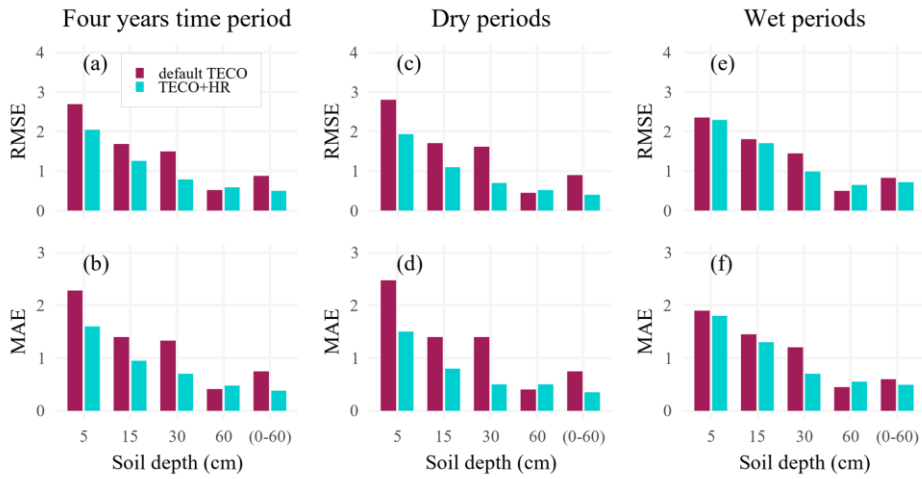
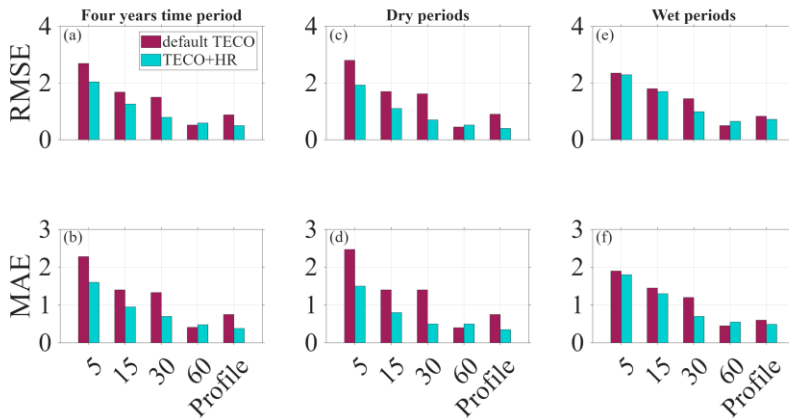


Figure 2: Model performance for soil moisture across different depths (5, 15, 30, and 60 cm, and 0-60 cm integrated soil profile), considering temporal variations in soil moisture conditions. Root Mean Square Error (RMSE) and Mean Absolute Error (MAE) are presented for the complete time series (a, b), dry periods (c, d), and wet periods (e, f). Lower values of RMSE and MAE indicate better model performance.

367



368

369

370

The data assimilation-constrained models, generally captured both the magnitude and dynamics of observational data, reproducing seasonal variations in soil moisture across four soil depths. Minor mismatches at the topsoil (5 cm) likely reflect the complexity of near-surface

371 processes that are not fully represented in simplified models and potential sensor lag due to
372 imperfect soil contact, as similar discrepancies are not observed at deeper layers. In addition,
373 following prolonged dry periods, initial rainfall can be largely offset by evaporation, resulting in
374 muted surface soil moisture responses (Miele et al., 2023; Cattry et al., 2025; Asadollahi et al.,
375 2022). While TECO+HR simulation showed an improvement in the overall model performance,
376 the impact of HR was mostly pronounced during dry periods (Figs. 1 and 2). We further
377 examined diurnal soil moisture fluctuations (Fig. S5) and found that TECO+HR ~~successfully~~
378 closely tracked~~reproduced~~ the observed diurnal cycles, whereas the default TECO failed to
379 capture this pattern, suggesting that the observed diurnal variability was likely driven by HR.
380 Additionally, we compared min-max normalized soil matric potential at 15, 30, and 60 cm with
381 simulations derived from Eq. (4) (Fig. S6). Both models reproduced the general trends of the
382 observations, suggesting that the simulated soil water potential gradients were consistent with
383 measurement.

384 Moreover, during periods of limited precipitation, the TECO+HR (blue lines) consistently
385 maintained higher soil moisture compared to default TECO (red lines), aligning closer to
386 observation particularly in the topsoil layers (Fig. 1a-c). Following precipitation events, the
387 default TECO and TECO+HR simulations converged, suggesting the minimal influence of HR
388 under wet conditions at the study site. However, as surface soil moisture decreased following
389 precipitation, the two simulations diverged again, with TECO+HR maintaining higher moisture
390 levels in the topsoil layers, highlighting the role of HR in maintaining soil moisture during
391 prolonged drought.

392 The incorporation of HR into TECO resulted in reductions in model errors. During dry
393 periods, the RMSE decreased by 25, 43, and 52% at 5, 15, and 30 cm soil depths, respectively.

394 However, limited improvement was observed at 60 cm soil depth. Correspondingly, the MAE
395 was reduced by 30, 53, and 60% at 5, 15, and 30 cm, respectively. Over the entire study period,
396 RMSE decreased by 24, 25, and 47% at 5, 15, and 30 cm, with MAE reductions were 29, 34, and
397 55% at the same depths (Fig. 2a-d). Overall soil profile performance improved as well, with
398 RMSE and MAE reductions over 40% for both the four-year simulation and dry periods. These
399 improvements during dry periods are especially important, as roots are most vulnerable to
400 drought. By mitigating soil water deficits in surface layers, HR could reduce the risk of hydraulic
401 failure, thereby supporting plant species survival and it could enable better prediction of
402 ecosystem responses to water stress, such as carbon uptake (Domec et al., 2010), and
403 evapotranspiration (Zhu et al., 2017). In contrast, during wet periods, HR had minimal influence
404 on soil moisture (Fig. 2e, f).

405 **3.3 Effect of HR on soil moisture**

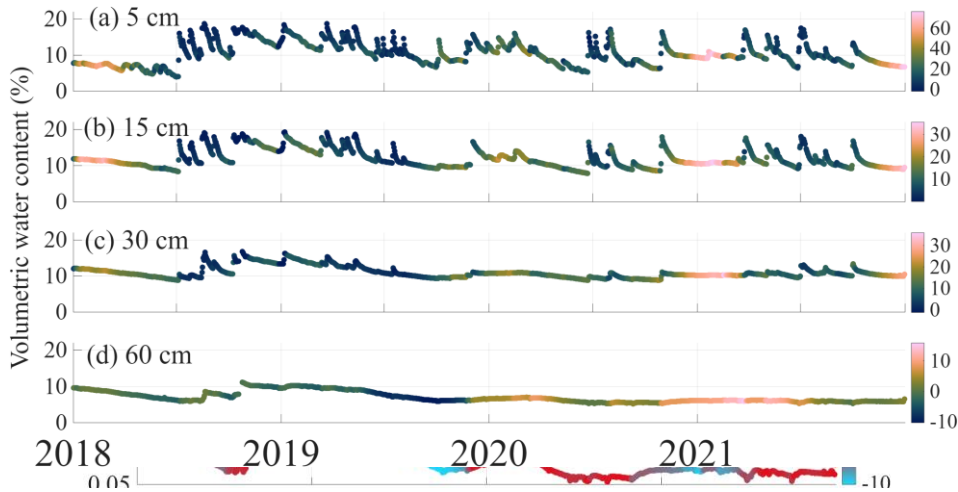


Figure 36: Relative change in modeled soil volumetric water content (SWC) (VWC%) compared to observed SWC across four soil depths (5, 15, 30, and 60 cm) depths. The color gradient represents the magnitude of relative change in modeled VSWC, calculated as $(HR - No\ HR) / No\ HR \times 100$, with HR and No HR indicating simulations with and without hydraulic redistribution, respectively. The relative change is overlaid on observed VWC."

- Formatted: Font: Italic
- Formatted: Font: Italic
- Formatted: Font: Italic
- Formatted: Font: Italic
- Formatted: Do not check spelling or grammar
- Formatted: Indent: First line: 0"

406
407 The direct impact of HR on hydrological processes should be evident in the soil profile
408 water content. We tested this by comparing VSWC model simulations in TECO with and
409 without HR processes, to observed VSWC time series at four depths (Fig. 36). We found that
410 cumulative effects of HR on soil moisture vary with depth, primarily due to the non-uniform root
411 biomass distribution throughout the soil profile (Fig. S8). The most pronounced effects of HR
412 were observed in the topsoil layers (5, 15, and 30 cm), where average daily water content
413 increased by up to 60% compared to simulation without HR. This increase was driven by upward
414 HR, especially during dry-down periods (Fig. 43b, and 6).

416 **3.3.3.4 HR simulations**

417 Model simulation revealed
418 distinct patterns of HR dynamics
419 across soil depths and temporal
420 scales. Fig. 43 illustrates these
421 patterns over two timescales: a short-
422 term, diurnal pattern (Fig. 43a), and a
423 long-term perspective from 2018 to
424 2021 (Fig. 43b). HR is a process with
425 both a source and a sink for water
426 movement. In the Fig. 43,
427 positive HR suggests that
428 a soil layer is gaining water (sink),
429 whereas negative HR values suggest
430 that the layer is losing water (source).

431 The short-term modeling analysis

432 highlights diurnal pattern of HR during dry conditions and a precipitation event (Fig. 43a). For
433 instance, on July 23, 2018, during a dry period, upward HR occurred, moving water from deeper
434 (> 100 cm) to shallower (0-30 cm) soil layers. However, following a precipitation event on July
435 24, 2018 (12 mm), this pattern shifted. The top 5 and 15 cm layers showed negative HR and a
436 decrease in the upward HR rate, respectively, acting as a water source for deeper layers. At the
437 same time, deeper soil layers showed a decline in negative HR rates, suggesting signs of
438 receiving water likely from the topsoil layers. The sum of HR across all soil layers remained

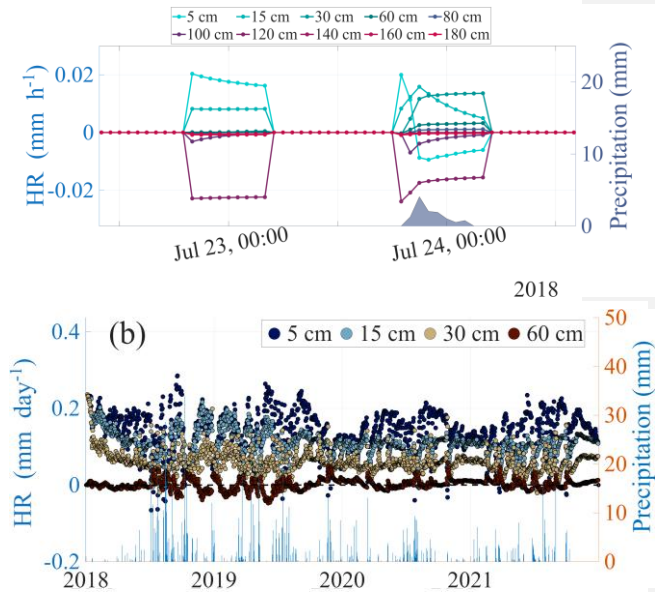


Figure 43: Temporal dynamics of hydraulic redistribution (HR). (a) diurnal pattern of modeled hydraulic HR redistribution across soil depths from July 22-24, 2018. The graph illustrates HR patterns during a dry period followed by a precipitation event (right y-axis). Colored lines represent different soil depths. (b) long-term daily HR trends and precipitation from January 2018 to December 2021. The blue shaded vertical bars represent precipitation (right y-axis).

439 zero, confirming that HR redistributed water rather than adding to the system. Consequently,
440 downward HR from the topsoil supplemented infiltration, enhancing water movement into
441 deeper soil layers, reflected by a decrease in the negative HR rates at depths and an increase in
442 the positive HR rate at 30 cm (Fig. 43a).

443 While our model simulates HR across 10 soil layers, we present long-term results for only
444 the top four soil layers (5, 15, 30, and 60 cm) to enable direct comparison with the available
445 observed soil moisture data. A clear seasonal pattern emerged, with HR generally intensifying
446 during dry periods (Fig. 43b).

447 Our model showed that upward HR was predominantly occurring in up to top 30 cm of soil
448 profile, with values ranging from -0.066 to 0.29 mm d^{-1} in each soil layer and an average of
449 0.30 mm d^{-1} across the top 30 throughout the study period. Downward HR, while less
450 pronounced, moved water only from the 5 cm soil layer during monsoon seasons and large
451 precipitation events (e.g., July 2018, 2019, 2020, and 2021; Fig. 43b). In contrast, 60 cm soil
452 layer typically exhibits a negative HR during dry periods, acting as a water source for upper
453 layers, and positive HR during wet periods, suggesting occasional water input from surface
454 layers ranging from -0.096 to 0.059 mm d^{-1} (mean 0.0015 mm d^{-1}). Moreover, integrated
455 soil profile (top 60 cm of soil profile), showed that upward HR was the dominant form of HR
456 throughout the year, ranging from 0.10 to 0.53 mm d^{-1} with a mean value 0.31 mm d^{-1} (Fig. S7).

457

458

459

460

Formatted: Superscript

461 **3.4.3.5 Precipitation influences on HR**

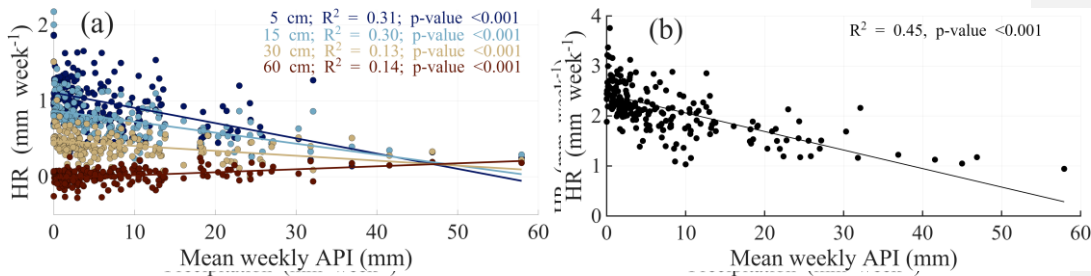


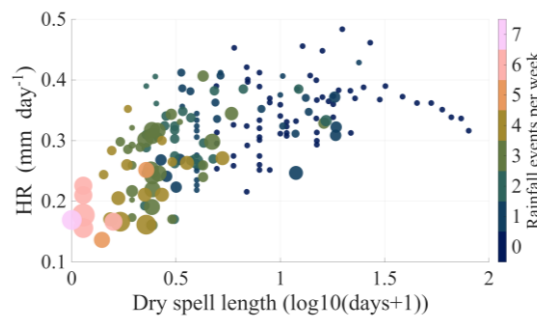
Figure 5-4: Relationships between *hydraulic redistribution (HR)* and *Antecedent Precipitation Index (API)*. (a) Weekly HR rates versus *mean weekly precipitation amounts API* at different soil depths (5, 15, 30, and 60 cm). *For each soil depth, the trend lines, and R², and corresponding p-values are shown for each depth.* (b) *Depth-integrated weekly HR across (0-60 cm) soil profile versus mean weekly precipitation API, with trend line, and R², and p-value.*

462 The model results showed a significant linear relationship between weekly HR and mean
 463 weekly precipitation API (mm-week⁻¹) (Fig. 5-4a-b). In the topsoil layers (5 cm and 15 cm), HR
 464 exhibited negative relationships with API ~~negative correlations were observed~~ (R² = 0.3140 and
 465 0.3028 respectively, both p-values < 0.001), indicating that HR activity decreased as antecedent
 466 moisture conditions became wetter. In contrast, positive correlation were observed at 30 and 60
 467 cm depths (R² = 0.13 and 0.14 respectively, both p-values < 0.001), suggesting downward
 468 redistribution under wetter antecedent conditions. ~~At the depth of 30 cm, a weak negative~~
 469 ~~correlation exists (R² = 0.07, p value < 0.05), suggesting a less pronounced reduction in HR rates~~
 470 ~~with increasing precipitation. Interestingly, at 60 cm depth, HR was positively correlated (R² =~~
 471 ~~0.16, p value < 0.001) with precipitation.~~

472 Additionally, when HR was integrated across the soil profile, a significant
 473 negative relationship with mean weekly API was observed (R² = 0.45, p-values < 0.001, Fig. 5b).
 474 This suggests that overall HR activity was greatest under drier antecedent conditions and
 475 declined as cumulative moisture availability increased, highlighting the stronger role of HR in
 476 regulating soil water dynamics during prolonged dry periods ~~when considering total HR across~~

477 the soil profile (0-60 cm), the modeled data showed a significant negative correlation with
 478 precipitation was observed ($R^2=0.31$, p -values < 0.001 , Fig. 4b). This suggests that overall HR
 479 activity decreased as precipitation increases, highlighting the stronger potential impact of HR on
 480 soil moisture during drier conditions.

481 However, despite these clear trends,
 482 variability in HR was observed across the
 483 full range of mean weekly API values we
 484 observed a considerable variability in HR
 485 was observed across the range of
 486 precipitation (Fig. 5a-b). This variability,



487 which could be attributed to the rainfall
 488 frequency, event size, and the duration of
 489 dry periods between rainfall events (Fig.
 490 65), factors that are implicitly captured by
 491 API. Figure 6 provides a more detailed view
 492 of these controls by relating HR directly to dry spell length and rainfall frequency, suggesting
 493 that HR may increase not only with reduced precipitation frequency but also as the interval
 494 between consecutive rainfall events lengths. HR. These results suggest that HR may increase not
 495 only with reduced precipitation frequency but also as the interval between consecutive rainfall
 496 events lengthen (Fig. 5). HR was lowest under conditions of high rainfall frequency and shorter
 497 dry spells, progressively increasing to its peak in the absence of rainfall. However, as the drought
 498 period extended beyond 30 days, HR declined, suggesting potential limitation on availability of
 499 deeper water to sustain HR. This variability is further illustrated through three scenarios (Fig.

Formatted: Font: Italic

Formatted: Font: Italic, Subscript

Formatted: Font: Italic

500 S7): 1) Following a rainfall event (28 mm on July 5, 2018), HR in the top 60 cm of soil profile
501 was minimal at 0.13 mm $d^{-1}d^{-1}$, indicating limited driving force for water redistribution when
502 soil moisture was abundant. 2) During a transition period between rainfall events (July 5-10,
503 2018), HR gradually increased but remained moderate, ranging from 0.13 to 0.20 mm $d^{-1}d^{-1}$,
504 suggesting a progressive activation of the redistribution process as soil began to dry. 3) During a
505 prolonged dry period (November 23-30, 2018), HR peaked at 0.20-0.52 mm $d^{-1}d^{-1}$,
506 demonstrating enhanced redistribution activity in response to the development of soil moisture
507 gradients.

508

509

510

511 4. Discussion

512 4.1 Patterns of hydraulic redistribution

513 Our findings support the hypothesis that upward HR is the dominant form of HR in dryland
514 ecosystems due to limited precipitation amount and sporadic rainfall events (Fig. S7). This
515 prevalence of upward water movement is characteristic of semi-arid regions, where deep-rooted
516 plants often redistribute water from moist deeper layers to drier surface soils during periods of
517 water stress (Caldwell et al., 1998; Ryel et al., 2002). Notably, the most pronounced HR
518 occurred in the topsoil layer (5, 15, and 30 cm), (Fig. 43b), which can be attributed to vertical
519 root distribution, with over 50% of root biomass concentrated in the top 30 cm ($D_{50} = 25$ cm) of
520 the soil profile (Fig. S8). Similar relationships between root distribution and HR intensity have
521 been reported in previous studies, where deeper root systems extend redistribution to deeper soil

522 layers, whereas shallow root systems amplify HR effects in surface soil due to higher root
523 density and activity. This pattern aligns with findings of (Hao et al., 2013b), which suggest that
524 deeper root distributions extend HR to deeper soil layers, while shallower root systems enhance
525 HR in the topsoil layers due to higher root density and activity (Fig. S8).

526 The magnitude of HR simulated in this study (0.10-0.53 mm d⁻¹ for top 60 cm soil) falls
527 within the range reported in previous studies. Estimated HR rates for the topsoil were
528 comparable to values synthesized in the global review by Neumann and Cardon (2012), which
529 reported HR magnitudes ranging from 0.04 to 3.2 mm d⁻¹ across ecosystem. However, our
530 estimates are slightly higher than the upper range reported by Yang et al. (2022) for desert or
531 sparsely vegetated ecosystems (0.014-0.475 mm d⁻¹). These differences likely reflect variations
532 in vegetation structure, rooting depth, soil texture, and water availability among ecosystems.

533
534 Our model simulations estimated HR rates in range 0.10-0.53 mm d⁻¹ for top 60 cm soil depth
535 (Fig. S7), values that fall within the broader range of 0.04 to 3.2 mm d⁻¹ reported in the
536 comprehensive review by Neumann and Cardon (2012) but exceed the upper limit of the 95%
537 confidence interval of 0.014-0.475 mm d⁻¹ reported by Yang et al. (2022) for desert or sparsely
538 vegetated ecosystems, which synthesized empirical observations and modeling estimates of
539 average water movement attributed to HR.

540 The direct impact of HR on hydrological processes should be evident in the soil profile water
541 content. We tested this by comparing SWC model simulations in TECO with and without HR
542 processes, to observed SWC time series at four depths (Fig. 6). We found that cumulative effects
543 of HR on soil moisture vary with depth, primarily due to the non-uniform root biomass

Formatted: Not Superscript/ Subscript

Formatted: Indent: First line: 0"

544 distribution throughout the soil profile (Fig. S8). The most pronounced effects of HR were
545 observed in the topsoil layers (5, 15, and 30 cm), where average daily water content increased by
546 up to 60% compared to simulation without HR. This increase was driven by upward HR,
547 especially during dry-down periods (Fig. 2b, and 6).

548

549

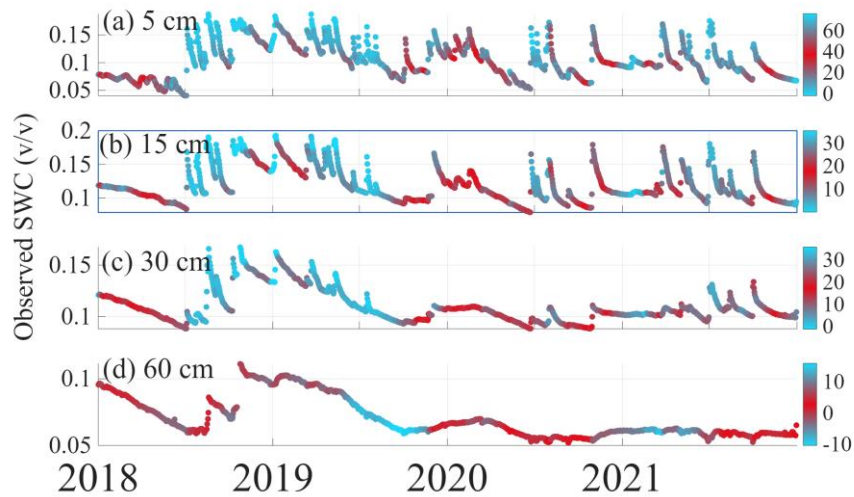


Figure 6: Relative change in soil water content (SWC) (%) compared to observed SWC at 5, 15, 30, and 60 cm depths. The color gradient represents the magnitude of relative change in SWC, calculated as $(HR - No\ HR) / No\ HR \times 100$, with HR and No HR indicating simulations with and without hydraulic redistribution."

550 4.2 Effects of precipitation variability on HR

551 Our findings support the hypothesis that the precipitation pattern significantly (p -value $<$
552 0.001) influences the magnitude and variability of HR (Figs. 43a-b, and S7). The rate of HR in
553 the topsoil profile (<60 cm) exhibited a consistent response pattern to precipitation events,
554 characterized by sharp decreases/declines following large rainfall, and a gradual recovery to pre-

555 rain levels during subsequent dry periods. Similar responses have been reported in previous
556 study, where precipitation temporarily suppresses HR by reducing water potential gradients
557 between shallow and deeper soil layers (Hao et al., 2013b). ~~These dynamics were particularly~~
558 ~~evident during years with frequent large precipitation events (2018-2019), where HR rates~~
559 ~~oscillated between 0.04 and 0.20 mm d⁻¹. For instance, after an 18 mm rainfall event on July 24,~~
560 ~~2018, HR rates dropped below 0.15 mm d⁻¹ before recovering to 0.30 mm d⁻¹ within 10 days.~~
561 ~~This pattern suggests a recharging effect: initially, infiltrating rainwater increases soil water~~
562 ~~potential in both shallow and deep layers, reducing the gradient between shallow and deep layers~~
563 ~~and temporarily suppressing HR (Hao et al., 2013b)~~. However, as water redistributes through the
564 soil profile, new hydraulic gradients ~~develop~~re-establish, leading to enhanced HR activity. In this
565 phase, roots actively redistribute water from newly moistened deep layers to drier shallow layers
566 (Yu and D'odorico, 2014; Ryel et al., 2002), ~~consistent with findings from (Yu and D'odorico,~~
567 ~~2014) and (Ryel et al., 2002)~~.

568 Our model predicted that HR rates were generally higher during rainless periods compared to
569 rainfall periods within a given year. For instance, during the prolonged dry period in 2020 (driest
570 year ~~with few small precipitation events~~), HR rates remained consistently high, 0.17-0.40 mm d⁻¹
571 ¹, with minimal fluctuations. The consistent high HR rates, likely arises from more pronounced
572 soil water potential gradients derived from sustained plant water demand and surface evaporation
573 in the absence of frequent precipitation (Fu et al., 2016; Meinzer et al., 2004).

574 Seasonal ~~trends~~patterns include higher HR rates (0.12-0.53 mm d⁻¹) during the drier periods
575 (typically from November to May) and lower rates (0.10-0.30 mm d⁻¹) during the monsoon
576 season (usually from June to October) (Fig. S7). This seasonality underscores the influence of
577 both precipitation patterns and potential evapotranspiration on HR dynamics, highlighting that

578 HR is likely more pronounced during drier seasons when soil moisture gradients are likely to be
579 more substantial due to reduced precipitation and potentially higher evaporative demand (Scott et
580 al., 2008; Fu et al., 2016; Yu and D'odorico, 2014).

581 **4.3 Limitation and future perspectives**

582 While our modeling study provides valuable insights into HR dynamics in PJ woodlands,
583 several limitations should be noted. (1) The model does not account for inter-annual changes in
584 vegetation cover or species composition. Variations in plant functional types and leaf area index
585 may influence soil moisture and HR, and incorporating these dynamics could improve long-term
586 simulations. (2) ~~We~~ Our analysis focused on the dominant tree species at ~~our~~ study site;
587 ~~however, but~~ other plant species may also benefit from water redistributed by these trees,
588 ~~potentially affecting-influencing~~ ecosystem water dynamics. (3) We did not include stem water
589 refilling or nighttime transpiration reported by Howard et al. (2009) ~~and~~ Neumann et al. (2014),
590 which ~~could may~~ influence the magnitude of HR. (4) Finally, future studies should address these
591 limitations and further could investigate explore the role of HR in regulating ecosystem
592 functions, such as carbon exchange and evapotranspiration, ~~and examine whether incorporating~~
593 ~~HR improves predictions of ecosystem carbon dynamics proportionally to its effects on soil~~
594 ~~water~~.

595 **5. Conclusions**

596 This study demonstrates the role of hydraulic redistribution (HR) in soil water dynamics in
597 piñon-juniper woodlands. By integrating HR processes and observations into the Terrestrial
598 Ecosystem Model (TECO) via data assimilation, we successfully constrained model soil
599 hydraulics parameters and improved simulations of soil water content across multiple depths,

600 particularly in shallow soil layers (0–30 cm) and during dry periods. ~~Our model results showed~~
601 ~~that HR rates vary with the length of dry spells between rainfall events, generally decreasing~~
602 ~~with increasing precipitation magnitude and frequency, with HR rates ranging from 0.10 to 0.50~~
603 ~~mm d⁻¹ as conditions transitioned from wet to dry.~~ Our model results indicate that HR rates vary
604 in response to the duration of dry spells between rainfall events. Generally, HR rates tend to
605 increase as soil becomes drier and decreases with increasing precipitation magnitude and
606 frequency. Across the wet to dry transition, HR rates exhibit a range of 0.10 to 0.50 mm d⁻¹.

Formatted: Superscript

607 Consequently, HR increased soil moisture in topsoil layers by up to 60% during dry periods,
608 with upward HR emerging as the dominant flux, especially in the top 30 cm. These findings
609 underscore the potential influence of HR during dry periods and highlight its role in sustaining
610 soil water availability for vegetation. Future research should explore how HR-mediated water
611 redistribution affects ecosystem functions including carbon exchange, and evapotranspiration.

612 6. Acknowledgments

613 This research is supported by US Department of Energy’s Office of Biological and
614 Environmental Research, Environmental System Science (ESS) Program (DE-SC0023514 to
615 WTP, MEL and YL) and the modeling effort used data collected with funding from the US
616 National Science Foundation (IOS 1557176 to MEL, WTP, and Susan Schwinning). Additional
617 support from US NSF grants (DEB 2242034, DEB 2406930, and DEB 2425290), the US
618 Department of Energy’s Terrestrial Ecosystem Sciences Grant DE-SC0023514, subcontract
619 CW55561 from Oak Ridge National Laboratory to Cornell University, and the “NYS Connects:
620 Climate Smart Farms & Forestry” project, funded by the USDA, the New York State Department
621 of Environmental Conservation, and the New York State Department of Agriculture and
622 Markets. This research is also part of AI-CLIMATE: “AI Institute for Climate-Land Interactions,

623 Mitigation, Adaptation, Tradeoffs and Economy”, funded by the USDA National Institute of
624 Food and Agriculture (NIFA), the NSF National AI Research Institutes Competitive Award (No.
625 2023-67021-39829) and Swiss National Foundation, Award#P500PN_206603 for their financial
626 support of this collaboration.

627 **7. Competing interests**

628 The authors declare no competing interests.

629 **8. Author contributions**

630 **AKC:** Conceptualization, Methodology, Data curation, Formal analysis, Writing - original draft.

631 **YZ:** Conceptualization, Writing - review & editing. **MC:** Writing - review & editing. **HD:**

632 Writing - review & editing, Data curation. **ML:** Conceptualization, Data curation, Supervision,

633 Writing - review & editing, Funding acquisition, Project administration. **WP:** Conceptualization,

634 Data curation, Supervision, Funding acquisition, Writing - review & editing. **YL:**

635 Conceptualization, Supervision, Project administration, Funding acquisition, Writing - review &
636 editing.

637 **9. Code availability**

638 The Terrestrial ECOSystem (TECO) model used in this paper is ~~available~~ archived on Zenodo

639 under on GitHub at https://github.com/aneeshchandel/TECO_HR.

640 <https://doi.org/10.5281/zenodo.18201820>.

641 **10. Data availability**

642 The data supporting the findings of this study are available within the manuscript. Additional
643 data may be available upon request from the corresponding author, subject to compliance with
644 relevant data protection and privacy regulations.

645 **11. Supporting Information**

646 Supporting information accompanying this manuscript is available as a separate Word file. It
647 includes supplementary figures referenced in the main text.

648 **References**

- 649 Alfieri, J. G., Anderson, M. C., Kustas, W. P., and Cammalleri, C.: Effect of the revisit interval
650 and temporal upscaling methods on the accuracy of remotely sensed evapotranspiration
651 estimates, *Hydrology and Earth System Sciences*, 21, 83-98, 10.5194/hess-21-83-2017,
652 2017.
- 653 Amenu, G. G. and Kumar, P.: A model for hydraulic redistribution incorporating coupled soil-
654 root moisture transport, *Hydrology and Earth System Sciences*, 12, 55-74, 10.5194/hess-
655 12-55-2008, 2008.
- 656 Asadollahi, M., Nehemy, M. F., McDonnell, J. J., Rinaldo, A., and Benettin, P.: Toward a
657 closure of catchment mass balance: Insight on the missing link from a vegetated
658 lysimeter, *Water Resources Research*, 58, e2021WR030698, 2022.
- 659 Barron - Gafford, G. A., Knowles, J. F., Sanchez - Cañete, E. P., Minor, R. L., Lee, E., Sutter,
660 L., Tran, N., Murphy, P., Hamerlynck, E. P., and Kumar, P.: Hydraulic redistribution
661 buffers climate variability and regulates grass - tree interactions in a semiarid riparian
662 savanna, *Ecohydrology*, 14, e2271, 2021.
- 663 Barron - Gafford, G. A., Sanchez - Cañete, E. P., Minor, R. L., Hendryx, S. M., Lee, E., Sutter,
664 L. F., Tran, N., Parra, E., Colella, T., and Murphy, P. C.: Impacts of hydraulic
665 redistribution on grass - tree competition vs facilitation in a semi - arid savanna, *New
666 Phytologist*, 215, 1451-1461, 10.1111/nph.14693, 2017.
- 667 Beer, C., Reichstein, M., Tomelleri, E., Ciais, P., Jung, M., Carvalhais, N., Rödenbeck, C.,
668 Arain, M. A., Baldocchi, D., and Bonan, G. B.: Terrestrial gross carbon dioxide uptake:
669 global distribution and covariation with climate, *Science*, 329, 834-838, 2010.
- 670 Bleby, T. M., Mcelrone, A. J., and Jackson, R. B.: Water uptake and hydraulic redistribution
671 across large woody root systems to 20 m depth, *Plant, cell & environment*, 33, 2132-
672 2148, 2010.
- 673 Brooks, R. H.: Hydraulic properties of porous media, Colorado State University 1965.
- 674 Caldwell, M. M., Dawson, T. E., and Richards, J. H.: Hydraulic lift: consequences of water
675 efflux from the roots of plants, *Oecologia*, 113, 151-161, 10.1007/s004420050363, 1998.
- 676 Campbell, G. S.: *Soil physics with BASIC: transport models for soil-plant systems*,
677 Elsevier 1985.
- 678 Cattray, M., Miele, F., Wang, S., Frutschi, M., and Rinaldo, A.: Evaluating nitrate removal and
679 travel times in a bare deciduous forest soil through a column tracer experiment, *Catena*,
680 258, 109204, 2025.
- 681 Clapp, R. B. and Hornberger, G. M.: Empirical equations for some soil hydraulic properties,
682 *Water resources research*, 14, 601-604, 1978.
- 683 Domec, J. C., King, J. S., Noormets, A., Treasure, E., Gavazzi, M. J., Sun, G., and McNulty, S.
684 G.: Hydraulic redistribution of soil water by roots affects whole-stand evapotranspiration

Formatted: Indent: Left: 0", Hanging: 0.5"

685 and net ecosystem carbon exchange, *New Phytol*, 187, 171-183, 10.1111/j.1469-
686 8137.2010.03245.x, 2010.

687 Eastburn, J. F., Campbell, M. J., Dennison, P. E., Anderegg, W. R., Barrett, K. J., Fekety, P. A.,
688 Flake, S. W., Huffman, D. W., Kannenberg, S. A., and Kerr, K. L.: Ecological and
689 climatic transferability of airborne lidar-driven aboveground biomass models in Piñon-
690 Juniper woodlands, *GIScience & Remote Sensing*, 61, 2363577, 2024.

691 Fabian, G. S., Sandra, J. B., William, A. H., Frederick, C. M., and Guillermo, G.: Hydraulic lift
692 in a Neotropical savanna: Experimental manipulation and model simulations,
693 *Agricultural and Forest Meteorology*, 150, 629-639, 10.1016/j.agrformet.2010.02.001,
694 2010.

695 Fu, C. S., Wang, G. L., Gouliden, M. L., Scott, R. L., Bible, K., and Cardon, Z. G.: Combined
696 measurement and modeling of the hydrological impact of hydraulic redistribution using
697 CLM4.5 at eight AmeriFlux sites, *Hydrology and Earth System Sciences*, 20, 2001-2018,
698 10.5194/hess-20-2001-2016, 2016.

699 Fu, C. S., Wang, G. L., Bible, K., Gouliden, M. L., Saleska, S. R., Scott, R. L., and Cardon, Z. G.:
700 Hydraulic redistribution affects modeled carbon cycling via soil microbial activity and
701 suppressed fire, *Global Change Biology*, 24, 3472-3485, 10.1111/gcb.14164, 2018.

702 Grünzweig, J. M., De Boeck, H. J., Rey, A., Santos, M. J., Adam, O., Bahn, M., Belnap, J.,
703 Deckmyn, G., Dekker, S. C., and Flores, O.: Dryland mechanisms could widely control
704 ecosystem functioning in a drier and warmer world, *Nature ecology & evolution*, 6, 1064-
705 1076, 2022.

706 Hafner, B. D., Hesse, B. D., Bauerle, T. L., and Grams, T. E.: Water potential gradient, root
707 conduit size and root xylem hydraulic conductivity determine the extent of hydraulic
708 redistribution in temperate trees, *Functional Ecology*, 34, 561-574, 2020.

709 Hao, X. M., Chen, Y. N., Guo, B., and Ma, J. X.: Hydraulic redistribution of soil water in
710 *Populus euphratica* Oliv. in a central Asian desert riparian forest, *Ecohydrology*, 6, 974-
711 983, 10.1002/eco.1338, 2013a.

712 Hao, X. M., Li, W. H., Guo, B., and Ma, J. X.: Simulation of the effect of root distribution on
713 hydraulic redistribution in a desert riparian forest, *Ecological research*, 28, 653-662,
714 2013b.

715 Hastings, W. K.: Monte Carlo sampling methods using Markov chains and their applications,
716 1970.

717 Hillel, D.: Introduction to environmental soil physics, Elsevier2003.

718 Hou, E., Litvak, M. E., Rudgers, J. A., Jiang, L., Collins, S. L., Pockman, W. T., Hui, D., Niu, S.,
719 and Luo, Y.: Divergent responses of primary production to increasing precipitation
720 variability in global drylands, *Glob Chang Biol*, 27, 5225-5237, 10.1111/gcb.15801,
721 2021.

722 Howard, A. R., Van Iersel, M. W., Richards, J. H., and Donovan, L. A.: Night - time
723 transpiration can decrease hydraulic redistribution, *Plant, Cell & Environment*, 32, 1060-
724 1070, 2009.

725 Hultine, K. R., Cable, W. L., Burgess, S. S. O., and Williams, D. G.: Hydraulic redistribution by
726 deep roots of a Chihuahuan Desert phreatophyte, *Tree Physiology*, 23, 353-360, DOI
727 10.1093/treephys/23.5.353, 2003.

728 Jiang, J., Huang, Y., Ma, S., Stacy, M., Shi, Z., Ricciuto, D. M., Hanson, P. J., and Luo, Y.:
729 Forecasting responses of a northern peatland carbon cycle to elevated CO₂ and a gradient

730 of experimental warming, *Journal of Geophysical Research: Biogeosciences*, 123, 1057-
731 1071, 10.1002/2017jg004040, 2018.

732 Katul, G. G. and Siqueira, M. B.: Biotic and abiotic factors act in coordination to amplify
733 hydraulic redistribution and lift, *The New Phytologist*, 187, 3-6, 2010.

734 Kohler, M. A. and Linsley, R. K.: Predicting the runoff from storm rainfall, US Department of
735 Commerce, Weather Bureau1951.

736 Lee, E., Kumar, P., Barron-Gafford, G. A., Hendryx, S. M., Sanchez-Cañete, E. P., Minor, R. L.,
737 Colella, T., and Scott, R. L.: Impact of hydraulic redistribution on multispecies vegetation
738 water use in a semiarid savanna ecosystem: An experimental and modeling synthesis,
739 *Water Resources Research*, 54, 4009-4027, 10.1029/2017wr021006, 2018.

740 Li, X., Wei, Y., and Li, F.: Optimality of antecedent precipitation index and its application,
741 *Journal of Hydrology*, 595, 126027, 2021.

742 Luo, Y. and Reynolds, J. F.: Validity of extrapolating field CO₂ experiments to predict carbon
743 sequestration in natural ecosystems, *Ecology*, 80, 1568-1583, 10.1890/0012-
744 9658(1999)080[1568:Voefce]2.0.Co;2, 1999.

745 Luo, Y. and Schuur, E. A. G.: Model parameterization to represent processes at unresolved
746 scales and changing properties of evolving systems, *Glob Chang Biol*, 26, 1109-1117,
747 10.1111/gcb.14939, 2020.

748 Marshall, L., Nott, D., and Sharma, A.: A comparative study of Markov chain Monte Carlo
749 methods for conceptual rainfall - runoff modeling, *Water Resources Research*, 40, 2004.

750 Meinzer, F. C., Brooks, J. R., Bucci, S., Goldstein, G., Scholz, F. G., and Warren, J. M.:
751 Converging patterns of uptake and hydraulic redistribution of soil water in contrasting
752 woody vegetation types, *Tree Physiology*, 24, 919-928, 10.1093/treephys/24.8.919, 2004.

753 Metropolis, N., Rosenbluth, A. W., Rosenbluth, M. N., Teller, A. H., and Teller, E.: Equation of
754 state calculations by fast computing machines, *The journal of chemical physics*, 21,
755 1087-1092, 1953.

756 Miele, F., Benettin, P., Wang, S., Retti, I., Asadollahi, M., Frutschi, M., Mohanty, B., Bernier -
757 Latmani, R., and Rinaldo, A.: Spatially explicit linkages between redox potential cycles
758 and soil moisture fluctuations, *Water Resources Research*, 59, e2022WR032328, 2023.

759 Mosegaard, K. and Sambridge, M.: Monte Carlo analysis of inverse problems, *Inverse problems*,
760 18, R29, 2002.

761 Nadezhdina, N., Ferreira, M. I., Conceição, N., Pacheco, C. A., Häusler, M., and David, T. S.:
762 Water uptake and hydraulic redistribution under a seasonal climate: long - term study in
763 a rainfed olive orchard, *Ecohydrology*, 8, 387-397, 2015.

764 Nadezhdina, N., David, T. S., David, J. S., Ferreira, M. I., Dohnal, M., Tesař, M., Gartner, K.,
765 Leitgeb, E., Nadezhdin, V., and Cermak, J.: Trees never rest: the multiple facets of
766 hydraulic redistribution, *Ecohydrology*, 3, 431-444, 2010.

767 Neumann, R. B. and Cardon, Z. G.: The magnitude of hydraulic redistribution by plant roots: a
768 review and synthesis of empirical and modeling studies, *New Phytol*, 194, 337-352,
769 10.1111/j.1469-8137.2012.04088.x, 2012.

770 Neumann, R. B., Cardon, Z. G., TESHARA - LEVYE, J., Rockwell, F. E., Zwieniecki, M. A.,
771 and Holbrook, N. M.: Modelled hydraulic redistribution by sunflower (*Helianthus*
772 *annuus* L.) matches observed data only after including night - time transpiration, *Plant*,
773 *Cell & Environment*, 37, 899-910, 2014.

774 Nicola, M. and Ram, O.: Rhizosphere water content drives hydraulic redistribution: Implications
775 of pore-scale heterogeneity to modeling diurnal transpiration in water-limited

776 ecosystems, *Agricultural and Forest Meteorology*, 312,
777 10.1016/j.agrformet.2021.108720, 2022.

778 Novick, K. A., Ficklin, D. L., Baldocchi, D., Davis, K. J., Ghezzehei, T. A., Konings, A. G.,
779 MacBean, N., Raoult, N., Scott, R. L., and Shi, Y.: Confronting the water potential
780 information gap, *Nature Geosci*, 15, 158-164, 2022.

781 Prävälje, R.: Drylands extent and environmental issues. A global approach, *Earth-Science*
782 *Reviews*, 161, 259-278, 2016.

783 Prieto, I., Armas, C., and Pugnaire, F. I.: Water release through plant roots: new insights into its
784 consequences at the plant and ecosystem level, *New Phytol*, 193, 830-841,
785 10.1111/j.1469-8137.2011.04039.x, 2012.

786 Priyadarshini, K. V. R., Prins, H. H. T., de Bie, S., Heitkönig, I. M. A., Woodborne, S., Gort, G.,
787 Kirkman, K., Ludwig, F., Dawson, T. E., and de Kroon, H.: Seasonality of hydraulic
788 redistribution by trees to grasses and changes in their water - source use that change
789 tree - grass interactions, *Ecohydrology*, 9, 218-228, 10.1002/eco.1624, 2016.

790 Quijano, J. C. and Kumar, P.: Numerical simulations of hydraulic redistribution across climates:
791 The role of the root hydraulic conductivities, *Water Resources Research*, 51, 8529-8550,
792 10.1002/2014wr016509, 2015.

793 Rawls, W. J., Brakensiek, D. L., and Saxton, K.: Estimation of soil water properties,
794 *Transactions of the ASAE*, 25, 1316-1320, 1982.

795 Romme, W. H., Allen, C. D., Bailey, J. D., Baker, W. L., Bestelmeyer, B. T., Brown, P. M.,
796 Eisenhart, K. S., Floyd, M. L., Huffman, D. W., and Jacobs, B. F.: Historical and modern
797 disturbance regimes, stand structures, and landscape dynamics in pinon-juniper
798 vegetation of the western United States, *Rangeland Ecology & Management*, 62, 203-
799 222, 2009.

800 Ryel, R., Caldwell, M., Yoder, C., Or, D., and Leffler, A.: Hydraulic redistribution in a stand of
801 *Artemisia tridentata*: evaluation of benefits to transpiration assessed with a simulation
802 model, *Oecologia*, 130, 173-184, 10.1007/s004420100794, 2002.

803 Saito, T., Fujimaki, H., Yasuda, H., and Inoue, M.: Empirical temperature calibration of
804 capacitance probes to measure soil water, *Soil Science Society of America Journal*, 73,
805 1931-1937, 2009.

806 Sardans, J. and Peñuelas, J.: Hydraulic redistribution by plants and nutrient stoichiometry: Shifts
807 under global change, *Ecohydrology*, 7, 1-20, 2014.

808 Schwinning, S., Litvak, M. E., Pockman, W. T., Pangle, R. E., Fox, A. M., Huang, C. W., and
809 McIntire, C. D.: A 3-dimensional model of *Pinus edulis* and *Juniperus monosperma* root
810 distributions in New Mexico: implications for soil water dynamics, *Plant Soil*, 450, 337-
811 355, 10.1007/s11104-020-04446-y, 2020.

812 Scott, R. L., Cable, W. L., and Hultine, K. R.: The ecohydrologic significance of hydraulic
813 redistribution in a semiarid savanna, *Water Resources Research*, 44,
814 10.1029/2007wr006149, 2008.

815 Seneviratne, S. I., Corti, T., Davin, E. L., Hirschi, M., Jaeger, E. B., Lehner, I., Orlowsky, B.,
816 and Teuling, A. J.: Investigating soil moisture-climate interactions in a changing climate:
817 A review, *Earth-Science Reviews*, 99, 125-161, 2010.

818 Tang, J., Riley, W. J., and Niu, J.: Incorporating root hydraulic redistribution in CLM 4.5:
819 Effects on predicted site and global evapotranspiration, soil moisture, and water storage,
820 *Journal of Advances in Modeling Earth Systems*, 7, 1828-1848, 2015.

- 821 Ukkola, A. M., De Kauwe, M. G., Roderick, M. L., Burrell, A., Lehmann, P., and Pitman, A. J.:
822 Annual precipitation explains variability in dryland vegetation greenness globally but not
823 locally, *Global Change Biology*, 27, 4367-4380, 2021.
- 824 Wei, L., Qiu, Z., Zhou, G., Zuecco, G., Liu, Y., and Wen, Y.: Soil water hydraulic redistribution
825 in a subtropical monsoon evergreen forest, *Science of The Total Environment*, 835,
826 155437, 10.1016/j.scitotenv.2022.155437, 2022.
- 827 Weng, E. and Luo, Y.: Soil hydrological properties regulate grassland ecosystem responses to
828 multifactor global change: A modeling analysis, *Journal of Geophysical Research:
829 Biogeosciences*, 113, 10.1029/2007jg000539, 2008.
- 830 Williams, M., Rastetter, E., Fernandes, D., Goulden, M., Wofsy, S., Shaver, G., Melillo, J.,
831 Munger, J., Fan, S. M., and Nadelhoffer, K.: Modelling the soil - plant - atmosphere
832 continuum in a Quercus - Acer stand at Harvard Forest: The regulation of stomatal
833 conductance by light, nitrogen and soil/plant hydraulic properties, *Plant, Cell &
834 Environment*, 19, 911-927, 1996.
- 835 Willmott, C. J. and Matsuura, K.: Advantages of the mean absolute error (MAE) over the root
836 mean square error (RMSE) in assessing average model performance, *Climate research*,
837 30, 79-82, 2005.
- 838 Wu, H., Fu, C., Wu, H., and Zhang, L.: Influence of the dry event induced hydraulic
839 redistribution on water and carbon cycles at five AsiaFlux forest sites: A site study
840 combining measurements and modeling, *Journal of Hydrology*, 587, 124979,
841 10.1016/j.jhydrol.2020.124979, 2020.
- 842 Xu, T., White, L., Hui, D., and Luo, Y.: Probabilistic inversion of a terrestrial ecosystem model:
843 Analysis of uncertainty in parameter estimation and model prediction, *Global
844 Biogeochemical Cycles*, 20, 10.1029/2005gb002468, 2006.
- 845 Yan, B. and Dickinson, R. E.: Modeling hydraulic redistribution and ecosystem response to
846 droughts over the Amazon basin using Community Land Model 4.0 (CLM4), *Journal of
847 Geophysical Research: Biogeosciences*, 119, 2130-2143, 10.1002/2014jg002694, 2014.
- 848 Yang, G., Huang, L., and Shi, Y.: Magnitude and determinants of plant root hydraulic
849 redistribution: A global synthesis analysis, *Frontiers in Plant Science*, 13, 918585, 2022.
- 850 Yu, K. L. and D'Odorico, P.: Climate, vegetation, and soil controls on hydraulic redistribution in
851 shallow tree roots, *Advances in Water Resources*, 66, 70-80,
852 10.1016/j.advwatres.2014.02.003, 2014.
- 853 Yu, T., Feng, Q., Si, J., Xi, H., Li, Z., and Chen, A.: Hydraulic redistribution of soil water by
854 roots of two desert riparian phreatophytes in northwest China's extremely arid region,
855 *Plant Soil*, 372, 297-308, 10.1007/s11104-013-1727-8, 2013.
- 856 Zhang, D., Madsen, H., Ridler, M. E., Kidmose, J., Jensen, K. H., and Refsgaard, J. C.:
857 Multivariate hydrological data assimilation of soil moisture and groundwater head,
858 *Hydrology and Earth System Sciences*, 20, 4341-4357, 2016.
- 859 Zheng, Z. and Wang, G.: Modeling the dynamic root water uptake and its hydrological impact at
860 the Reserva Jaru site in Amazonia, *Journal of Geophysical Research: Biogeosciences*,
861 112, 2007.
- 862 Zhu, S., Chen, H., Zhang, X., Wei, N., Shangguan, W., Yuan, H., Zhang, S., Wang, L., Zhou, L.,
863 and Dai, Y.: Incorporating root hydraulic redistribution and compensatory water uptake
864 in the Common Land Model: Effects on site level and global land modeling, *Journal of
865 Geophysical Research: Atmospheres*, 122, 7308-7322, 2017.

866